INTERNATIONAL JOURNAL FOR NUMERICAL METHODS IN BIOMEDICAL ENGINEERING
*Int. J. Numer. Meth. Biomed. Engng.* 2012; **28**:1043–1055
Published online 25 August 2012 in Wiley Online Library (wileyonlinelibrary.com). DOI: 10.1002/cnm.2509

# Evaluation of carotid stent scaffolding through patient-specific finite element analysis

F. Auricchio [1,2], M. Conti [1,*,†], M. Ferraro [1,2] and A. Reali [1]

[1] *Dipartimento di Ingegneria Civile ed Architettura, Università degli Studi di Pavia, Via Ferrata 1, 27100 Pavia, Italy*
[2] *Center for Advanced Numerical Simulations (CESNA), Istituto Universitario di Studi Superiori di Pavia (IUSS), V.le Lungo Ticino Sforza 56, 27100 Pavia, Italy*

SUMMARY

After carotid artery stenting, the plaque remains contained between the stent and the vessel wall, moving consequently physicians' concerns toward the stent capability of limiting the plaque protrusion, that is, toward vessel scaffolding, to avoid that some debris is dislodged after the procedure. Vessel scaffolding is usually measured as the cell area of the stent in free-expanded configuration, neglecting thus the actual stent configuration within the vascular anatomy. In the present study, we measure the cell area of four different stent designs deployed in a realistic carotid artery model through patient-specific finite element analysis. The results suggest that after deployment, the cell area change along the stent length and the related reduction with respect to the free-expanded configuration are functions of the vessel tapering. Hence, the conclusions withdrawn from the free-expanded configuration appear to be qualitatively acceptable for comparative purposes, but they should be carefully handled because they neglect the post-implant variability, which seems to be more pronounced in open-cell designs, especially at the bifurcation segment. Even though the investigation is limited to few stent designs and one vascular anatomy, our study confirms the capability of dedicated computer-based simulations to provide useful information about complex stent features as vessel scaffolding. Copyright © 2012 John Wiley & Sons, Ltd.

Received 11 January 2012; Revised 5 July 2012; Accepted 3 August 2012

KEY WORDS: finite element analysis (FEA); carotid artery stenting (CAS); patient-specific modeling

## 1. INTRODUCTION

Cardiovascular diseases (CVDs) are nowadays the leading cause of death in the Western countries: a recent report of the American Heart Association [1] states that, on the basis of 2006 mortality rate, nearly 2300 Americans die of CVD each day, that is, an average of one death every 38 s. These data explain well the high incidence of such pathologies, leading to high social and economical costs (i.e., $ 503.2 billion per year).

Among CVDs, stroke[‡] has a significant incidence; approximately every 40 s, someone in the USA has a stroke. The pathologic events that lead to a stroke are complex, but most of them can be referred to atherosclerosis, a degeneration of the arterial wall, characterized by accumulation of cells, lipids, connective tissue, calcium, and other substances inside its inner layers resulting in the so-called atheroma or plaque. Atherosclerosis is the potential source of a number of events, ranging from arterial hardening to narrowing of the vessel lumen, that is, stenosis, which can lead to blockage

*Correspondence to: Michele Conti, Dipartimento di Ingegneria Civile ed Architettura, Università di Pavia, Via Ferrata 1, 27100 Pavia, Italy.

[†] E-mail: michele.conti@unipv.it

[‡] Sudden diminution or loss of consciousness, sensation, and voluntary motion, caused by rupture or obstruction (as by a clot) of a blood vessel of the brain.

of the blood flow. Atherosclerosis of the aorta and in particular of carotid artery (CA) is one of the main causes of stroke.

Several treatment options are nowadays available for managing CA stenosis, but thanks also to the encouraging outcomes achieved in the coronary district, the application of percutaneous minimally-invasive techniques, such as stenting, is rapidly arising. Carotid artery stenting (CAS) is a procedure that restores the vessel patency by enlarging the narrowed lumen through the expansion of a metallic mesh, driven to the target lesion in a catheter, running inside an endoluminal path accessed by groin incision.

Carotid artery stenting is a younger technology than its surgical counterpart, the so-called carotid endarterectomy. Whereas during carotid endarterectomy, the complete plaque is removed, with CAS, the plaque remains contained between the stent and the vessel wall, moving consequently the physicians' concerns from the intra-procedural to the post-procedural stage. In fact, stent struts compress the dilated plaque material, which should not protrude into the lumen to guarantee that no debris is dislodged after the procedure.

Starting from this basic concept, it is clear that the procedure outcomes are linked to stent design, which is usually resulting as a trade-off between several biomechanical features. Among others, the vessel scaffolding, that is, the stent capability to support the vessel wall after stenting, represents a crucial issue. Vessel scaffolding is usually determined by the free cell area, which is dependent upon the number and arrangement of bridge connectors. In closed-cell stents, adjacent ring segments are connected at every possible junction, whereas in open-cell stents, not all of the junction points are interconnected. Thus, a closed-cell stent design has a smaller cell area than its corresponding open-cell counterpart. The relation between stent design and procedure outcomes is still a matter of an intense clinical debate [2–6], recently extensively discussed and reviewed by Hart and colleagues [7].

The evaluation of vessel scaffolding is not easily standardized or measured; typically, the cell area of a given stent is measured in its free-expanded configuration [8]. Although this measure is appropriate to compare different designs, it is challenging to be measured *in vivo* and does not take into account the actual configuration of a stent implanted in a tortuous carotid bifurcation. This limitation can be overcome exploiting realistic simulations of CAS [9].

Within this framework, the present study aims at assessing the cell area of four different stent designs deployed in a realistic CA model through patient-specific finite element analysis (FEA).

## 2. MATERIALS AND METHODS

In this section, we start from our previous study [9], addressing the validation of CAS simulation with respect to a real stent deployed in a patient-specific silicon mock artery. We then combine the methodologies proposed in that paper with a procedure to measure the cell area in order to accomplish the goal of the present study.

### *2.1. Vessel model*

The patient-specific vessel model considered in this study is reflecting the geometry of a silicon mock artery, derived from DICOM images of a neck–head computed tomography angiography performed on an 83-year-old male patient at IRCCS San Matteo in Pavia, Italy. The common carotid artery has a mean diameter of 7 mm whereas the internal carotid artery has a mean diameter of 5.2 mm; a mild stenosis (24% based on NASCET method) is present slightly above the bifurcation.

Given the variable wall thickness of the silicon model, the related finite element model is derived by a high-resolution micro-CT scan of the sole mock artery, segmented by Mimics v.13 (Materialise, Leuven, Belgium). For the sake of simplicity, only a portion with a length of 42 mm, meshed by 73322 10-node modified tetrahedron with hourglass control - C3D10M - elements and 134092 nodes, of the whole model (Figure 1) is considered for the simulation performed by Abaqus/Explicit v. 6.10 (Dassault Systèmes, Providence, RI, USA), as discussed in Section 2.3.



DOI: 10.1002/cnm

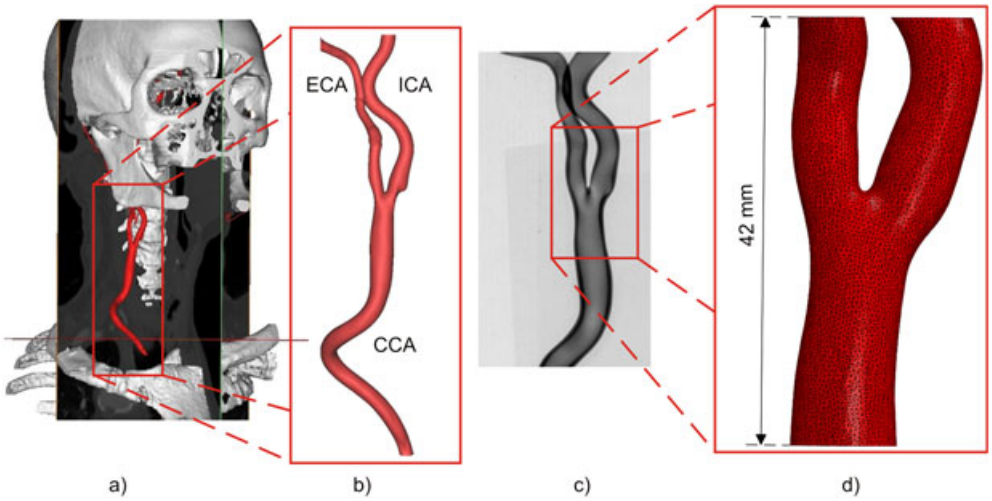


Figure 1. Elaboration of computed tomography angiography images: (a) whole 3D reconstruction of neck–head district highlighting the region of interest; (b) surface describing the carotid artery lumen used to create the silicon artery; (c) radiography of the silicon artery highlighting the non-uniform wall thickness; (d) tetrahedral mesh adopted in the simulations.

The mechanical response of silicon is reproduced assuming a hyperelastic material model, defined by a second-order polynomial strain energy potential $U$ defined as:

$$U = \sum_{i+j=1}^{2} C_{ij}(\bar{I}_1 - 3)^i(\bar{I}_2 - 3)^j + \sum_{i=1}^{2} \frac{1}{D_i}(J^{el} - 1)^{2i} \tag{1}$$

where $C_{ij}$ and $D_i$ are material parameters; $\bar{I}_1$ and $\bar{I}_2$ are respectively the first and second deviatoric strain invariants. The material model calibration is performed on the stress–strain data derived from a tensile test on a silicon sample and results in the following non-null coefficients: $C_{10} = -2.40301$ MPa; $C_{01} = 3.02354$ MPa; $C_{20} = 0.456287$ MPa; $C_{11} = -1.72892$ MPa; $C_{02} = 2.73598$ MPa.

### 2.2. *Stent finite element model*

Four different self-expanding Nitinol carotid stent designs are considered. They resemble four commercially available stents used in the clinical practice. In the following, they will be referred to as model A (ACCULINK - Abbott, Illinois, USA), model B (Bard ViVEXX Carotid Stent - C. R. Bard Angiomed GmbH & Co., Germany), model C (XACT - Abbott, Illinois, USA) and model D (CRISTALLO Ideale - Invatec/Medtronic, Roncadelle (BS), Italy), respectively. Given the comparative nature of the study, for all designs, we considered the straight configuration having a 9 mm reference diameter and 30 mm length. Because no data are available from the manufacturer, the main geometrical features of such devices are derived from high-resolution micro-CT scans of the stent in the delivery system (Figure 2(a)). As discussed in previous studies [9, 10], the stent model to be embedded in CAS simulation is generated through the following steps:

- a planar CAD geometry (Figure 2(b)), corresponding to the unfolding of stent crimped in the delivery catheter, is generated by Rhinoceros v. 4.0 SR8 (McNeel and Associated, Seattle, WA, USA) and subsequently imported to Abaqus/CAE v. 6.10 (Dassault Systèmes, Providence, RI, USA) where the mesh is generated;
- through appropriate geometrical transformations performed by an in-house code in Matlab (The Mathworks Inc., Natick, MA, USA), the planar mesh is *rolled* leading to the final crimped stent (i.e., laser-cut configuration) as depicted in Figure 2(c);



DOI: 10.1002/cnm

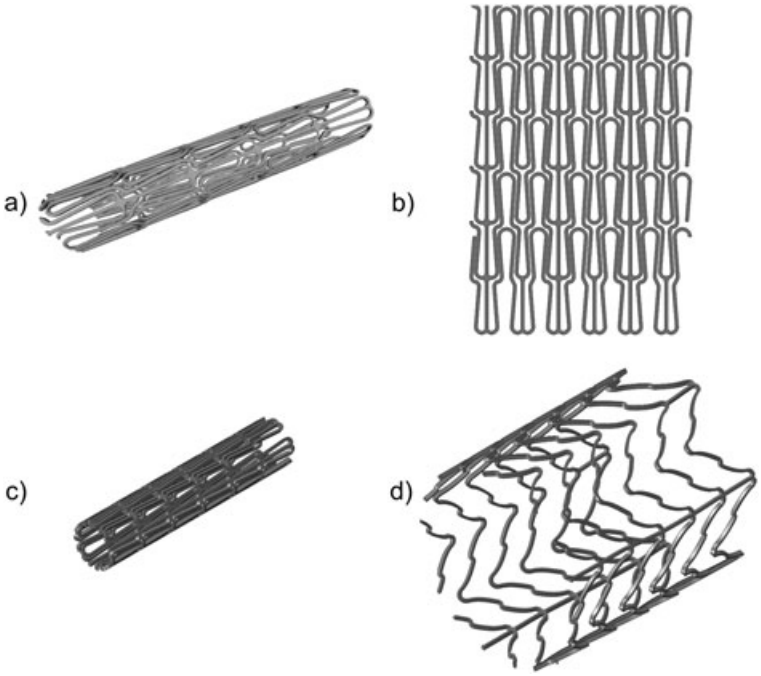


Figure 2. Stent mesh generation: (a) detail of a high resolution micro-CT performed on a real stent within the delivery system; (b) planar CAD geometry resembling the stent design pattern); (c) stent mesh in crimped configuration; (d) stent mesh in free-expanded configuration.

Table I. Overview of analyzed stents. The hybrid stent has closed-cell design in the mid part and an open-cell design at the ends.

| Model label | A | B | C | |
|---|---|---|---|---|
| Reference stent Design | ACCULINK Open-cell | VIVEXX Open-cell | XACT Closed-cell | CRISTALLO Hybrid |
| N° cells | | | | |
| $Proximal_1$ | 6 | 15 | 18 | 5 |
| $Proximal_2$ | 3 | 5 | 18 | 5 |
| $Bifurcation_1$ | 3 | 5 | 18 | 14 |
| $Bifurcation_2$ | 3 | 5 | 18 | 14 |
| $Distal_1$ | 3 | 5 | 18 | 5 |
| $Distal_2$ | 9 | 15 | 18 | 5 |
| N. Elements | 90552 | 78160 | 74764 | 30000 |
| N. Nodes | 177066 | 41144 | 33948 | 65010 |

- simulating the shape-setting process through FEA (solver: Abaqus/Explicit v. 6.10 - Dassault Systèmes, Providence, RI, USA), the crimped configuration is transformed into the free-expanded configuration (see Figure 2(d)).

The mesh details about the considered stent FE models are reported in Table I, where also the numbers of the considered cells for the area measurement, with respect to three stent segments (i.e., proximal, bifurcation and distal), are reported. The stent models in free-expanded configurations are instead depicted in Figure 3.

### *2.3. Stent deployment simulation*

To investigate the interaction between the stent and the patient-specific CA model, we perform a two-step simulation procedure [9, 11]. In the first step, the diameter of the stent is decreased



DOI: 10.1002/cnm

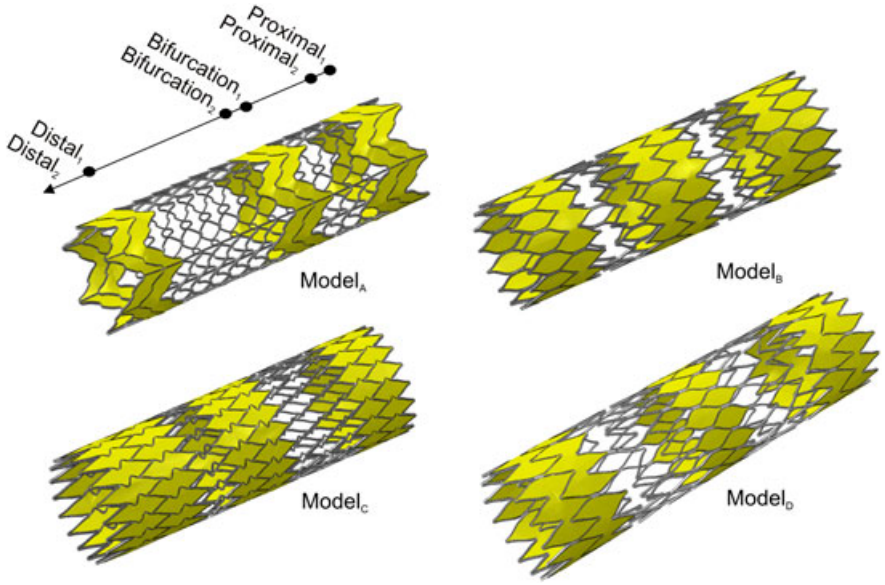


Figure 3. Considered stent designs in free-expanded configuration. The cells considered for area computation are depicted in yellow.

simulating the loading phase of the stent into the delivery system. Subsequently, the stent inside the delivery sheath is placed into the target lesion and there the retractable sheath is removed allowing stent/vessel interaction and thus mimicking stent placement. We use the pre-stenting vessel centerline for stent positioning, and the stent deformation is imposed by a profile change of the retractable sheath, through appropriate displacement boundary conditions on its nodes. These boundary conditions are determined as the difference between the starting and final sheath shape. The simulation is performed using Abaqus/Explicit v. 6.10 as finite element solver, because the numerical analysis is characterized by non-linearity due to the material properties, large deformations and complex contact problems. The general contact algorithm is used to handle the interactions between all model components; in particular, a frictionless contact between the stent and delivery sheath, and a friction coefficient of 0.2 between the stent and the vessel inner surface is assumed.

The superelastic behavior of Nitinol is modeled using the Abaqus user material subroutine [12], and the related constitutive parameters are obtained from the literature [13]; we consider such material properties identical for all stents, and we assume the density to be 6.7 g/cm$^3$.

### 2.4. *Measuring the stent cell area*

We measure the cell area of a 3D surface having the cell contour as a boundary. To create such a surface, it is necessary to: (i) identify the cell boundary nodes; (ii) sort these nodes in an appropriate manner to define a spline; (iii) use the spline to create the target surface. To speed up such a process, we integrate Matlab and Rhinoceros in a workflow defined by the following steps:

1. *Node set identification of each cell boundary from the planar mesh*: because the node label does not change along the geometrical transformation described in Section 2.2, we move from the planar mesh to clearly identify cell boundary nodes and to easily associate the related nodal labels (Figure 4(a) and (b)).
2. *Delaunay triangulation of each node set*: the basic idea is to use the triangulation (Figure 4(c)) to detect the outer edges and the related nodes, using thus the edge connectivity to drive the nodal sorting. The procedure is improved by the introduction of user-defined *dummy* nodes in order to have less distorted triangle elements inside the cell, improving the efficiency of the next step.



DOI: 10.1002/cnm

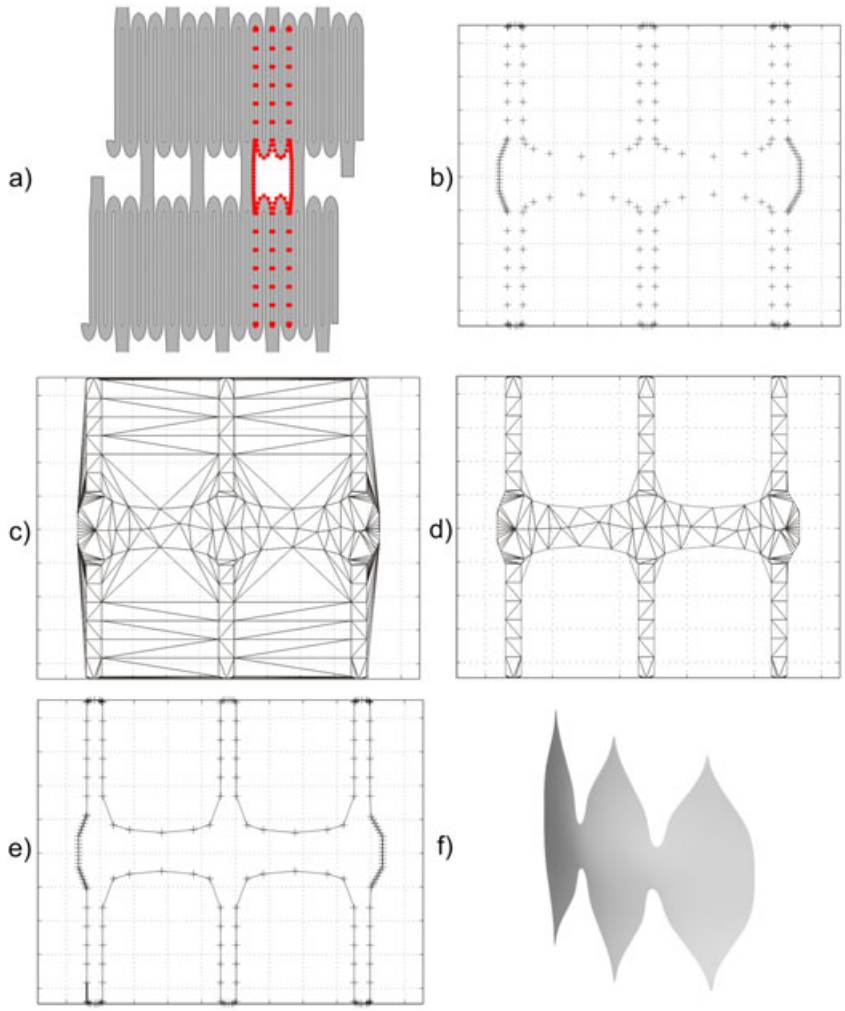


Figure 4. Cell surface definition: (a) and (b) Node identification of cell boundary nodes; (c) Delaunay triangulation of each node set; (d) Delaunay triangulation after the application of distortion criterion; (e) detection of outer edges; (f) and creation of 3D cell surface.

3. *Detection of outer edges and node sorting*: as depicted in Figure 4(c), the mesh obtained in the previous step does not match the cell boundaries. To overcome such a problem, we exploit the approach proposed by Cremonesi *et al*. [14], taking advantage of a distortion criterion to remove the unwanted triangles. In particular, for each triangle of the mesh, the shape factor is defined as $\alpha_e = (R_e/h) \geq (1/\sqrt{3})$, where $R_e$ is the radius of the circumcircle of the $e$th triangle and $h$ the minimal distance between two nodes in the element. This factor represents an index for element distortion and can be used after the setting of a proper threshold, to remove the unwanted triangles without any modification of the original Delaunay triangulation. For this work, to create an algorithm able to change its requirement with the different cell configurations, we set the shape threshold to $1.5\,\overline{\alpha_e}$, where $\overline{\alpha_e}$ is the $\alpha_e$ average. After the undesired cells removal (Figure 4(d)), the algorithm identifies the cell borders (Figure 4(e)) and sorts the nodal labels to make them suitable for the next step. At this stage, the nodal labels can be associated with the deformed nodal coordinates to obtain the deformed cell.
4. *Creation of a 3D surface for each cell and area measuring*: through a script in Rhinoceros, we firstly define a third-order polynomial curve passing through the cell boundary nodes, and we finally create the related patch surface, as illustrated in Figure 4(f). In this way, each cell area can be automatically measured and exported in a tabular format.



DOI: 10.1002/cnm

Table II. Comparison of cell area obtained using our approach with respect to the data reported by Müller-Hülsbeck *et al*. [8], considered here as a reference. Data are reported as the mean ± standard deviation; $mm^2$ is the unit of measure.

| | ACCULINK 7-10 × 30 $mm^2$ | | XACT 8-10 × 30 $mm^2$ | | Cristallo 7-10 × 30 $mm^2$ | |
|---|---|---|---|---|---|---|
| Stent segment | Model | Ref. | Model | Ref. | Model | Ref. |
| $Proximal_1$ | $8.7 \pm 0.1$ | | $3.3 \pm 0.1$ | 3.1 | $15.8 \pm 0.1$ | 13.5 |
| $Proximal_2$ | $16.3 \pm 0.0$ | 16.6 | $3.2 \pm 0.1$ | | $16.3 \pm 0.2$ | |
| $Bifurcation_1$ | $15.1 \pm 0.0$ | 15.1 | $3.7 \pm 0.1$ | 3.55 | $3.4 \pm 0.1$ | 3.3 |
| $Bifurcation_2$ | $15.5 \pm 0.0$ | | $3.6 \pm 0.1$ | | $3.3 \pm 0.1$ | |
| $Distal_1$ | $12.7 \pm 0.1$ | 13.6 | $4.8 \pm 0.1$ | 4.0 | $11.7 \pm 0.1$ | 12.4 |
| $Distal_2$ | $3.8 \pm 1.2$ | | $4.9 \pm 0.1$ | | $11.1 \pm 0.1$ | |

In this study, we compute the cell area as a scaffolding measure because it resembles in a more accurate manner the current configuration of the cell with respect to other comparators such as the largest fitted-in circle, which would somehow represent the maximum size of a plaque particle potentially protruding through the stent struts. With respect to this issue, Müller-Hülsbeck *et al*. [8] report a largest fitted-in circle of 1.18 mm for both ACCULINK (open-cell) and XACT (closed-cell) and 1.2 mm CRISTALLO Ideale (closed-cell) in the corresponding stent middle portion, whereas the cell area is 15.10 $mm^2$ for ACCULINK, 3.55 $mm^2$ for XACT and 3.30 $mm^2$ for CRISTALLO. From these data, we can observe that LFC does not catch the difference between the various stent designs that is instead particularly evident through the cell area.

## 3. RESULTS

To evaluate the suitability of our approach, we have firstly compared the cell areas computed in free-expanded configuration by our numerical models with respect to the data available in the literature. Given the lack of studies dealing with this topic, for such a comparison, we can only refer to the work of Müller-Hülsbeck *et al*. [8]. In particular, for our purpose, we consider the measurements reported about (i) 7-10 × 30 mm[§] ACCULINK (Abbott, Illinois, USA), (ii) 8-10 × 30 mm XACT (Abbott, Illinois, USA) and (iii) 7-10 × 30 mm CRISTALLO Ideale (Invatec/Medtronic, Roncadelle (BS), Italy). Because the considered stents are tapered, we appropriately modify Models A, C and D during the shape-setting step of stent mesh creation. As highlighted in Table II, our results are acceptably matching the experimental data. We remark that in Table II, the data from Müller-Hülsbeck *et al*. [8] of distal and proximal segments have been swapped, because we believe that a typo is present in that paper. Such a consideration is reasonable if we assume that, given the same cell shape, the smaller the diameter of the related segment, the smaller is the cell area; consequently, in a tapered stent, the distal segment diameter is smaller than the proximal one and thus the corresponding cell area. With respect to Model D, we would also underline that our results match well with the data presented by Cremonesi *et al*. [15], who are in fact reporting an average cell area of 15.17 $mm^2$ for the proximal segment, 3.24 $mm^2$ for the middle segment and 11.78 $mm^2$ for the distal one.

The post-stenting configurations obtained by the deployment simulations with respect to the four considered models are reported in Figure 5. Given the free-expanded and deployed configuration, for each stent, it is possible to compute the cell area with respect to four stent segments as reported in Table III and Figure 6.

Both Models A and B are generally classified as *open-cell*, but at distal and proximal ends, the cells are partially closed in Model A and fully closed in Model B, to enhance the stent stability during the release; this feature is not present on Model D. Considering the free-expanded configuration, this aspect leads to a variable cell size in the distal and proximal segment as highlighted in Figure 6, whereas the cell area is uniform in the bifurcation segment. After the deployment, if we

[§]distal-proximal diameter × length.



DOI: 10.1002/cnm

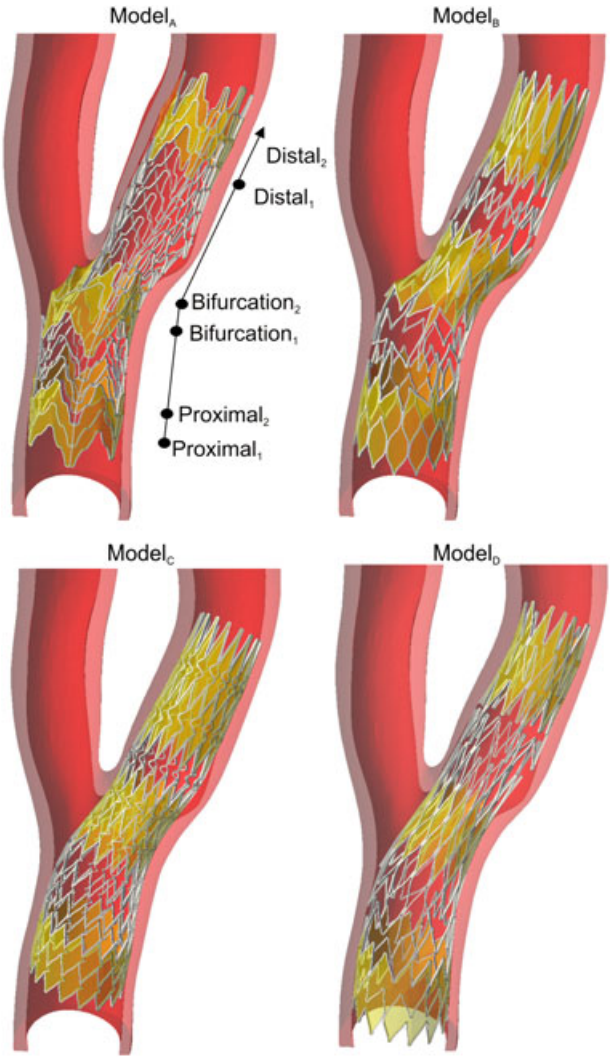


Figure 5. Considered stent designs after the deployment simulation. The cells considered for area computation are depicted in yellow.

consider the cell sets ranging from $Proximal_2$ to $Distal_1$, it is possible to notice that the cell area is decreasing following the vessel tapering pointing up the dependence of the cell size from the target vessel caliber. For Model B, it is worth to notice that the percentage reduction of different cell types is comparable in the proximal and distal segments (Table III).

Model C, which is a fully closed-cell design, shows a peculiar behavior. In fact, it has a cell shape varying along the length, leading to a progressive cell size increase, which is evident in free-expanded configuration (Figure 6(c)). This feature compensates the cell area reduction due to apposition, providing thus a uniform cell size after the deployment.

Model D resembles the features of Cristallo Ideale carotid stent, a nitinol self-expanding stent, which has a hybrid design consisting of three segments: a closed cell midsection with open cell portions at both edges, which are intended to provide adequate scaffolding to the carotid plaque while assuring high flexibility and vessel wall adaptability. Such a variability in the design is reflected by the change of the cell area along the stent length, showing a smaller cell area in the bifurcation segment.

Analyzing the standard deviation values, it is possible to notice that the vessel curvature induces a non uniform distribution of the cell area in circumferential direction for Models A and B especially



DOI: 10.1002/cnm

Table III. Cell area in free-expanded configuration and after the stent deployment. Data are reported as the mean ± standard deviation; $mm^2$ is the unit of measure.

| Model label | Configuration | $Proximal_1$ | $Proximal_2$ | $Bifurcation_1$ | $Bifurcation_2$ | $Distal_1$ | $Distal_2$ |
|---|---|---|---|---|---|---|---|
| Model A | Free exp. | 7.7±0.2 | 16.4±0.5 | 15.4±0.4 | 15.1±0.2 | 16.2±0.3 | 4.8±1.7 |
| | Implanted | 6.3±0.4 | 12.6±0.9 | 12.0±5.9 | 9.4±2.2 | 7.5±0.8 | 2.4±0.9 |
| | Implanted versus free exp. (%) | −18.2 | −23.1 | −22.2 | −38.1 | −53.4 | −49.1 |
| Model B | Free exp. | 4.1±0.0 | 13.4±0.0 | 13.7±0.0 | 13.9±0.0 | 13.3±0.0 | 4.1±0.0 |
| | Implanted | 3.5±0.1 | 11.6±0.6 | 9.0±1.2 | 8.7±0.8 | 7.1±0.1 | 2.3±0.2 |
| | Implanted versus free exp. (%) | −13.7 | −13.7 | −34.2 | −37.1 | −46.3 | −44.3 |
| Model C | Free exp. | 3.0±0.0 | 3.0±0.0 | 3.7±0.0 | 3.7±0.0 | 5.1±0.0 | 5.4±0.0 |
| | Implanted | 2.6±0.4 | 2.5±0.2 | 2.2±0.3 | 2.2±0.1 | 2.8±0.3 | 2.6±0.4 |
| | Implanted versus free exp. (%) | −13.9 | −15.2 | −39.0 | −40.8 | −44.5 | −51.4 |
| Model D | Free exp. | 14.2±0.1 | 14.8±0.2 | 3.5±0.1 | 3.5±0.1 | 14.5±0.3 | 14±0.1 |
| | Implanted | 12.1±0.6 | 12.3±0.8 | 2.2±0.4 | 2.1±0.3 | 6.7±0.2 | 6.4±0.3 |
| | Implanted versus free exp. (%) | −14.8 | −16.8 | −43.4 | −44.1 | −53.9 | −54.7 |

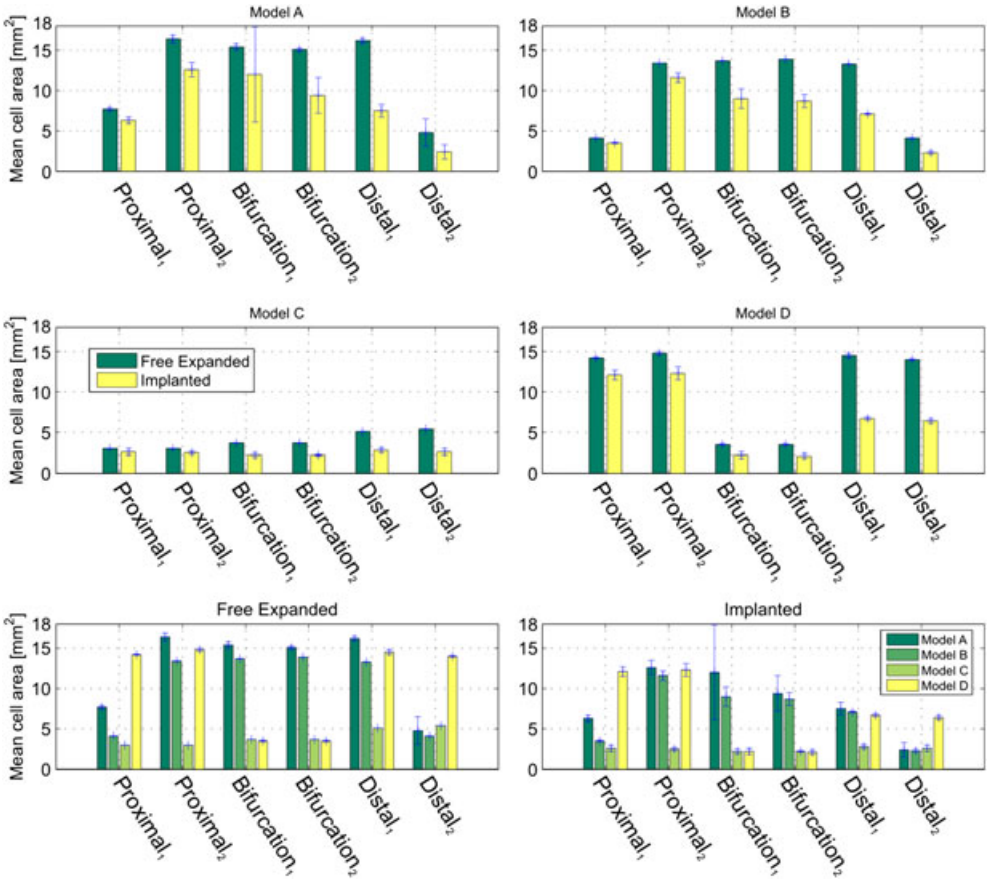


Figure 6. Bar graph of the mean cell area: free expanded versus implanted for each stent model (top and middle); comparison between the stent models in free-expanded configuration (bottom-left) and implanted (bottom-right).



DOI: 10.1002/cnm

in the bifurcation segment. This effect is particularly evident for Model A (Figure 5(a)), where the bending due to the angulated CA bifurcation, causes a misalignment and protrusion of the stent struts on the open surface, so-called fish-scaling effect.

The indications provided by the free-expanded configuration (Figure 6(e)) are qualitatively maintained after the deployment (Figure 6-bottom); in fact, Model A has the larger cell areas whereas Models C and D have the smaller ones at the bifurcation level. It is necessary to underline that in the segment $Distal_2$, the cell area of Model D is higher than the other stent models, but by a clinical point of view, this aspect is negligible because often, the middle part of the stent is in charge to cover the plaque.

## 4. DISCUSSION

Carotid angioplasty and stenting is usually inducing the disruption of atheromatous plaque obstructing the lumen. Consequently, the physicians' concerns are now turned to stent capability to limit plaque protrusion, that is, vessel scaffolding, to avoid that some debris is dislodged after the procedure.

There is an intense debate [2–7, 16, 17] about the impact of stent design on post-procedural events. Hart *et al*. [6] by a retrospective study suggest that patients treated with closed-cell stents have a lower risk to experience post-procedure adverse events, when compared to patients treated with open-cell design; they formulate the hypothesis that because transient ischemic attack is related to small particles passing through the stent mesh, closed-cell stents have a superior capability to scaffold the emboligenic plaque given to their smaller free cell area.

Bosiers *et al*. [5] support the conclusions from Hart *et al*. [6], showing that post-procedural complication rates are higher for the open-cell stent types, especially in symptomatic patients; moreover, such complications increase with larger free cell area. Consequently, Bosiers *et al*. [18] sustain that the smaller the free cell area, the better is the stent capability to keep plaque material behind the struts. Although, the characteristics of the plaque and its stability should be considered for an appropriate patient selection [19]

Schillinger *et al*. [4] do not confirm the indications previously illustrated; in fact, their retrospective analysis has not indicated any superiority of a specific carotid stent cell design with respect to neurological complications, stroke, and mortality risk.

This debate has been further enriched by other contributions [2, 3, 7] highlighting the need of other dedicated studies.

Given such considerations, it is possible to state that stent scaffolding is a clinically relevant topic; unfortunately, the clinical debate has not an *engineering* counterpart. In particular, really few studies are addressing the quantification of vessel scaffolding of a given stent design. Müller-Hülsbeck *et al*. [8] performed an *in vitro* study measuring the cell area of several commercially available stents in free-expanded configuration. They performed the measurements by the software of their optical microscope. Despite the fact that this approach is appropriate for comparative purposes, it neglects the current configuration of the stent implanted in a tortuous CA bifurcation and the related cell configuration change. In our previous study [9], we have considered only one stent model in two design configurations, using the interstrut angle as a measure of scaffolding. Consequently, it is clear that there is still room for further investigations; hence, we measure the cell area of four different stent designs deployed in a realistic CA model through patient-specific FEA.

Our results confirm the basic idea that, given a cell shape, the cell area depends on the size of the vessel segment where the stent is deployed. Even if this result is not surprising, it is important to underline that there is a dramatic reduction of the cell size (up to $-54.7\%$) after the deployment. Despite the fact that the indications derived from the free-expanded configuration are useful and appropriate for comparative purposes, the conclusions withdrawn by this approach should be carefully considered; in fact, they neglect the variance of the cell size along the stent length, which sometimes mitigates the difference between two stent designs observed in the free-expanded state. Following these thoughts, we agree with Siewiorek *et al*. [20], who sustain that analyses on the basis of binary classification, such as open-cell versus closed-cell, or on a single variable may be misleading, given the complexity of the approached problem.



DOI: 10.1002/cnm

Our results also confirm the qualitative observation reported by Wholey and Finol [21], who underline the role of vessel anatomy for vessel scaffolding; in fact, when cells open on the concave surface of an angulated CA bifurcation, they could prolapse showing the so-called fish scaling effect. This issue could induce some drawbacks and is affecting the scaffolding uniformity at the bifurcation segment (Figures 5 and 6(d)).

## 5. LIMITATIONS

The main limitations of the present study are related to the following items: (i) only one specific vascular anatomy is considered; and (ii) the degree of stenosis is low (i.e., 24%). The consideration of more severe stenosis demands for the assessment of the atherosclerotic plaque morphology and its mechanical response, which is one of the most challenging within the framework of stenting simulations. In particular, the mechanisms driving the plaque rupture during pre-stenting angioplasty should be accounted and modeled; in fact, during real CAS procedure approaching severe stenosis, the vessel patency is primarily restored with an angioplastic procedure and after that, the stent is deployed to avoid elastic recoil leading to early re-occlusion.

Up to now, the majority of the numerical studies addressing structural analysis of stent in atherosclerotic vessel does not consider severe stenosis [11, 22, 23] and simplifies the problem from both geometrical and constitutive points of view [24, 25]. Despite the fact that an excellent study toward realistic investigation of stenting in highly stenotic (iliac) artery was already provided by Holzapfel and colleagues in 2005 [26], the inclusion of micro-damage and damage mechanism, occurring in the arterial wall due to vascular injury during angioplasty and stent deployment, is still an open point. In this context, it is worth to mention the contribution of Ferrara and Pandolfi [27], who simulated the arterial crack propagation induced by mechanical actions through cohesive surfaces; despite the fact that such a methodology seems very appealing, it calls for the support of deep experimental investigations, able to provide the necessary data (geometrical, material constant for elasticity and fracture) and thus not easy to implement, especially in a patient-specific case.

Given such considerations and the comparative nature of the present study, we believe that the consideration of a mild stenosis is acceptable. However, future consideration of more severe degrees of stenosis would strengthen the relation between the obtained results and the clinical practice. Moreover, it is necessary to highlight that in the present study, we do not consider the impact of plaque morphology and stability on the vessel scaffolding, because we focus mainly on its relationship with the stent design *per se*. A low/mild stenosis can be more dangerous than a severe one if the plaque is vulnerable; this issue is in fact related to post-stenting plaque prolapse and is a matter of concern during the procedure planning and for the patient eligibility [28]. Nevertheless, such a simplification is consistent with the experimentally validated simulation presented in [9], which has shown the ability to predict the deformed configuration of a real stent deployed in a silicon mock artery.

## 6. CONCLUSIONS

In the present study, we measure the cell area of three different stent designs deployed in a realistic CA model through patient-specific FEA with the aim to consider the actual configuration of the stent within the vessel. The results suggest that after the deployment, the cell area change along the stent length and the related reduction with respect to the free-expanded configuration are functions of the vessel tapering. Nevertheless, for comparative purposes, the conclusions withdrawn from the free-expanded configuration appear to be qualitatively acceptable, but they should be carefully handled because they do not take into account the variability affecting the cell area distribution after the implant. Such a variability seems to be more pronounced in open-cell designs, whose scaffolding uniformity is impaired especially at the bifurcation segment.

Even though the investigation is limited to few stent designs and one vascular anatomy, our study confirms the capability of dedicated simulations based on computational mechanics methods,



DOI: 10.1002/cnm

such as FEA, to provide useful information about complex stent features as vessel scaffolding. Such predictions could be used to design novel carotid stents or for pre-surgical planning purposes.

ACKNOWLEDGEMENTS

This work is supported by the European Research Council through the FP7 Ideas Starting Grant project no. 259229 and by the Cariplo Foundation through the Project no. 2009.2822.

The authors would like to acknowledge Dr. R. Dore, Prof. A. Odero, and Dr. S. Pirrelli of IRCCS Policlinico S. Matteo, Pavia, Italy for their support on medical aspects related to the present work; Eng. D. Van Loo of Ghent University (UGCT), Ghent, Belgium for micro-CT scanning of stent samples.

REFERENCES

1. AHA committee. Heart disease and stroke statistics 2010 update: a report from the American Heart Sssociation. *Circulation* 2010; **121**:e46–e215.
2. Cremonesi A, Setacci C, Castriota F, Valgimigli M. Carotid stent cell design: lack of benefit or lack of evidence? *Stroke* 2009; **39**:e130.
3. Setacci C, de Donato G, Bosiers M. Two different studies on carotid stent cell design importance, or are we just saying the same thing? *Stroke* 2008; **39**:e129.
4. Schillinger M, Gschwendtner M, Reimers B, Trenkler J, Stockx L, Mair J, Macdonald S, Karnel F, Huber K, Minar E. Does carotid stent cell design matter? *Stroke* 2008; **39**:905–909.
5. Bosiers M, de Donato G, Deloose K, Verbist J, Peeters P, Castriota F, Cremonesi A, Setacci C. Does free cell area influence the outcome in carotid artery stenting? *European Journal of Vascular and Endovascular Surgery* 2007; **33**:135–141.
6. Hart J, Peeters P, Verbist J, Deloose K, Bosiers M. Do device characteristics impact outcome in carotid artery stenting? *Journal of Vascular Surgery* 2006; **44**:725–730.
7. Hart J, Bosiers M, Deloose K, Uflacker R, Schönholz C. Impact of stent design on the outcome of intervention for carotid bifurcation stenosis. *The Journal of Cardiovascular Surgery* 2010; **51**:799–806.
8. Müller-Hülsbeck S, Schäfer P. J, Charalambous N, Schaffner S, Heller M, Jahnke T. Comparison of carotid stents: an in vitro experiment focusing on stent design. *Journal of Endovascular Therapy* 2009; **16**:168–177.
9. Conti M, Van Loo D, Auricchio F, De Beule M, De Santis G, Verhegghe B, Pirrelli S, Odero A. Impact of carotid stent cell design on vessel scaffolding: a case study comparing experimental investigation and numerical simulations. *Journal of Endovascular Therapy* 2011; **18**:397–406.
10. Conti M, Auricchio F, De Beule M, Verhegghe B. Numerical simulation of Nitinol peripheral stents: from laser-cutting to deployment in a patient specific anatomy. *Proceeding of ESOMAT 2009* 2009:06008. DOI: 10.1051/esomat/200906008.
11. Auricchio F, Conti M, De Beule M, De Santis G, Verhegghe B. Carotid artery stenting simulation: from patient-specific images to finite element analysis. *Medical Engineering & Physics* 2011; **33**:281–289.
12. Rebelo N, Walker N, Foadian H. Simulation of implantable stents. *Abaqus User's Conference* 2001; **143**:421–434.
13. Kleinstreuer C, Li Z, Basciano C, Seelecke S, Farber M. Computational mechanics of Nitinol stent grafts. *Journal of Biomechanics* 2008; **41**:2370–2378.
14. Cremonesi M, Frangi A, Perego U. A Lagrangian finite element approach for the analysis of fluid-structure interaction problems. *International Journal for Numerical Methods in Engineering* 2010; **84**(5):610–630.
15. Cremonesi A, Rubino P, Grattoni C, Scheinert D, Castriota F, Biamino G. Multicenter experience with a new hybrid carotid stent. *Journal of Endovascular Therapy* 2008; **15**:186–192.
16. Tadros R, Spyris C, Vouyouka A, Chung C, Krishnan P, Arnold M, Marin M, Faries P. Comparing the embolic potential of open and closed cell stents during carotid angioplasty and stenting. *Journal of Vascular Surgery* 2012; **56**(1):89–95. DOI: 10.1016/j.jvs.2011.12.077.
17. Cremonesi A, Gieowarsingh S, Castriota F. Choice of the stent: Does the type of stent influence the outcome of carotid artery angioplasty and stenting? In *The Carotid and Supra-Aortic Trunks: Diagnosis, Angioplasty and Stenting*, Henry M, Diethrich EB, Polydorou A (eds), (2nd Edn). Wiley-Blackwell: Oxford, UK, 2011, DOI: 10.1002/9781444329803.ch27.
18. Bosiers M, Deloose K, Verbist J, Peeters P. What practical factors guide the choice of stent and protection device during carotid angioplasty? *European Journal of Vascular and Endovascular Surgery* 2008; **35**:637–643.
19. Bosiers M, Deloose K, Peeters P. Plaque stability and carotid stenting. In *Practical Carotid Artery Stenting*, Macdonald S, Stansby G (eds). Springer: London, 2009; 81–92.
20. Siewiorek G, Wholey M, Finol E. In vitro performance assessment of distal protection filters: pulsatile flow conditions. *Journal of Endovascular Therapy* 2009; **16**:735–743.
21. Wholey M, Finol E. Designing the ideal stent. *Endovascular Today* 2007; **6**:25–34.
22. Mortier P, Holzapfel G, De Beule M, Van Loo D, Taeymans Y, Segers P, Verdonck P, Verhegghe B. A novel simulation strategy for stent insertion and deployment in curved coronary bifurcations: comparison of three drug-eluting stents. *Annals of Biomedical Engineering* 2010; **38**:88–99.

23. Wu W, Qi M, Liu X, Yang D, Wang W. Delivery and release of Nitinol stent in carotid artery and their interactions: a finite element analysis. *Journal of Biomechanics* 2007; **40**:3034–3040.
24. Gastaldi D, Morlacchi S, Nichetti R, Capelli C, Dubini G, Petrini L, Migliavacca F. Modelling of the provisional side-branch stenting approach for the treatment of atherosclerotic coronary bifurcations: effects of stent positioning. *Biomechanics and Modeling in Mechanobiology* 2010; **9**(5):551–561.
25. Lally C, Dolan F, Prendergast P. Cardiovascular stent design and vessel stresses: a finite element analysis. *Journal of Biomechanics* 2005; **38**:1574–1581.
26. Holzapfel G, Stadler M, Gasser T. Changes in the mechanical environment of the stenotic arteries during interaction with stents: computational assessment of parametric stent design. *Journal of Biomechanical Engineering* 2005; **127**:166–180.
27. Ferrara A, Pandolfi A. Numerical modelling of fracture in human arteries. *Computer Methods in Biomechanics and Biomedical Engineering* 2008; **11**(5):553–567.
28. Gillard J, Graves M, Hatsukami T, Yuan C. *Carotid Disease, the Role of Imaging in Diagnosis and Management*. Cambridge University Press: Cambridge, United Kingdom, 2007.



DOI: 10.1002/cnm